communications biology

Article

https://doi.org/10.1038/s42003-025-07462-9

NLRP3 promotes inflammatory signaling and IL-1β cleavage in acute lung injury caused by cell wall extract of *Lactobacillus casei*

Lingui Gu[1,4], Jinjin Zhu[1,4], Qingbing Nie[1,4], Binghua Xie[2], Shuo Xue[1], Ailing Zhang[1], Qiangwei Li[1], Zhengzhong Zhang[3], Shupeng Li[1], Yusen Li[1], Qinquan Shi[1], Weiwei Shi[1], Lei Zhao[2] ✉, Shuzhen Liu[1] ✉ & Xuanming Shi[1] ✉

Gram-positive bacterial pneumonia is a significant cause of hospitalization and death. Shortage of a good experimental model and therapeutic targets hinders the cure of acute lung injury (ALI). This study has established a mouse model of ALI using Gram-positive bacteria *Lactobacillus casie* cell wall extracts (LCWE) and identified the key regulator NLRP3. We show that LCWE induces TNF, NF-κB signaling, and so on pathways. Similar to lipopolysaccharide (LPS), LCWE induces the infiltration of CD11b-positive cells and inflammation in lungs. LCWE also triggers inflammatory signaling through TLR2, different from LPS through TLR4. It suggests that cytokines amplify inflammation signaling relying on NLRP3 in LCWE-induced ALI. NLRP3 deletion disrupts inflammation, IL-1β cleavage, and the infiltration of neutrophils and macrophages in the injured lung. Our study highlights an animal ALI model for Gram-positive bacterial pneumonia and that NLRP3 is a key therapeutic target to prevent inflammation and lung damage in LCWE-induced ALI.

Pneumonia is a common cause of ALI and acute respiratory distress syndrome (ARDS), leading to significant hospitalizations and deaths among adults[1,2]. Pathogens of pneumonia include bacteria, viruses, mycobacteria, fungi, and parasites[3–6]. Bacteria are the primary pathogens of pneumonia, categorized as community-acquired and hospital-acquired pneumonia[3]. One of the most common bacteria is *Streptococcus pneumoniae*[1,2], a Gram-positive bacterium. In addition, secondary bacterial infections play a critical role following viral infection. Gram-positive bacteria such as *Staphylococcus aureus* and *S. pneumoniae* were the main pathogens after severe influenza infection, historically causing morbidity and mortality[7–9].

S. aureus activates inflammatory signaling pathways during lung infections. The nucleotide-binding oligomerization domain containing 2 (Nod2) functions as a sensor to detect muramyl dipeptide (MDP), a common unit of peptidoglycan found in most Gram-positive bacteria[10]. Loss of Nod2 reduced lung inflammation and neutrophil recruitment induced by *S. aureus*[11]. Ahn et al. discovered that IL-16 contributes to *S. aureus* infection through tumor necrosis factor receptor (TNFR) in $CD4^+$ cells[9]. In mouse lungs and THP-1 monocytes, the inflammasome protein NLRP3 is essential for activated inflammation[12]. Gram-positive bacteria activate the expression of inflammasome proteins like NLRC4, which reduces IL-17A-dependent neutrophil accumulation in Gram-positive pneumonia[13]. During infection, the bacterial cell wall is the first part to interact with host cells. However, it remains unknown whether and how the cell wall of Gram-positive bacteria contributes to lung inflammation and ALI.

The murine model of ALI facilitates uncovering molecular mechanisms underlying ARDS[14,15]. In recent years, LPS from Gram-negative bacteria has been used to induce inflammatory responses in animal models by inhalation administration, establishing an ALI mouse model[16,17]. Lipoteichoic acid (LTA) has been mentioned in a few studies but is not widely used due to an unestablished model. In addition, global changes in gene expression and signaling pathways in ALI induced by Gram-positive and Gram-negative bacteria are yet to be determined. The Gram-positive bacteria *Lactobacillus casie* cell wall extract (LCWE) is widely used as an inducer of the autoimmune disease IgA vasculitis[18]. As cell wall components of *L. casie* are similar to the ones of the primary ALI pathogen *S. aureus*, we

[1]The School of Basic Medical Sciences, Anhui Medical University, Hefei, Anhui, 230023, P. R. China. [2]The Fuyang Hospital, Anhui Medical University, Fuyang, Anhui, 236000, P. R. China. [3]The First Affiliated Hospital, Anhui Medical University, Hefei, Anhui, 230023, P. R. China. [4]These authors contributed equally: Lingui Gu, Jinjin Zhu, Qingbing Nie. ✉e-mail: ayefyzhaolei@163.com; szliu8@hotmail.com; xuanming.shi@hotmail.com

wonder if LCWE of *L. casie* can induce lung inflammation and acute lung injury to facilitate the identification of therapeutic target.

In this study, we established a murine model of ALI induced by LCWE to uncover how Gram-positive bacteria induce lung inflammation and to determine the key therapy targets for ALI/ARDS. Our data suggested that LCWE induced inflammation signaling pathway through TLR2, and MYD88 relays the signaling to activate NF-κB signaling pathways. Loss of NLRP3 disrupted inflammatory gene expression of IL6, TNFα, and pro-IL-1β in THP-1 cells and LCWE-induced ALI lung, highlighting NLRP3 as the therapeutic target of Gram-positive bacterial pneumonia.

Results

LCWE induces severe ALI

To determine whether Gram-positive bacteria *Lactobacillus casie* cell wall extract (LCWE) induces ALI, we administered LCWE to mouse lungs and collected lung tissues for pathological analysis. LPS, derived from Gram-negative bacteria and known as an ALI inducer, was used for positive control, and PBS was applied for vehicle control. Hematoxylin and Eosin (H&E) staining showed that the alveoli were evenly distributed in the control lungs (Fig. 1A). Compared to the vehicle control groups, the LPS-treated groups have smaller alveoli. The lungs were infiltrated with more immune cells (Figs. 1A, S1A), possibly causing the disappearance of the alveoli. These observations were consistent with previous reports of ALI[14,19,20]. Surprisingly, in the LCWE-treated groups, some lung regions were infiltrated with massive immune cells, and the alveoli disappeared completely, suggesting severe lung injury was induced by LCWE. Pathological analyses showed that the lung injury score induced by LCWE was comparable to that induced by LPS (Fig. 1B). As the marker genes of Toll/NF-κB signaling, total IL-1β and IL-10 faithfully reflect inflammation status and were used for a readout of inflammation[21,22]. Both LPS and LCWE induced a significant increase in *Il1b* and *Il10* mRNA (Fig. 1C). Altogether, LCWE induces comparable lung injury and inflammation to LPS. Subsequently, we compared the effects of LCWE and LPS on ALI at doses 1, 3, and 6 mg/kg (Fig. S1B–D). Consistently, all three different doses (1, 3, and 6 mg/kg) of LPS and LCWE induced severe ALI according to pathological analysis, and dramatic expression increase of IL-1β (Fig. 1D) and IL-10 proteins (Fig. 1E) in the injured lung tissues by immunostaining and both in the injured lung tissues and bronchoalveolar lavage fluid (BALF) by ELISA (Fig. 1F). These assays suggested that LCWE, the cell wall of Gram-positive bacteria, induces severe ALI, and inflammation in lung infection.

LCWE induces Toll/NF-κB and TNF signaling and promotes T cell differentiation in ALI

To understand the global changes of gene expression in our well-established LCWE- and LPS-induced ALI mouse models, we performed transcriptomic analyses on lung tissues with ALI (Fig. 2A, B). LPS altered the mRNA expression of 1884 genes, while LCWE did 5592 genes. The 897 upregulated genes by LPS were involved in TNF, Toll-like receptor, and NF-κB signaling pathways in KEGG pathway enrichment analysis (Fig. S2-A). In contrast, besides TNF, the Toll-like receptor signaling pathways, the IL-17 pathway was specifically activated by LCWE within the top signaling pathways of the 2043 genes (Fig. S2-B). Since both LCWE and LPS induce ALI, we analyzed the 792 overlapping upregulated genes to identify commonly activated signaling pathways during ALI. The confirmed top signaling pathways were TNF, Toll-like receptor, and NF-κB pathways (Fig. 2C, D). In addition, LCWE activated T cell differentiation into Th1, Th2, and Th17 subsets (Fig. 2E). The GO (Gene Ontology) analysis of differentially expressed genes indicated that the overlapped biological processes included leukocyte migration, immune effector functions, inflammatory response, and toll-like receptor binding (Fig. S3). Pathways related to calcium, cAMP signaling were downregulated by both LPS and LCWE, LCWE alone and LPS alone (Fig. S4). We further verified the mRNA expression of NF-κB pathway genes including *Nfkbia*, *Myd88*, *Tnfa*, and *Il6* in ALI by quantitative PCR. All these genes were significantly upregulated by both LPS and LCWE stimulation (Fig. 3). The expression of CD14, the cofactor of TLR4, was significantly activated by LPS, consistent with the previous report[23]. The interferon pathway genes *Stat6*, *Irf7*, T cell activation regulator gene *Saa3*, and chemokine genes *Cxcl2* and *Cxcl3* were strongly activated by LCWE and LPS (Fig. 3), suggesting that LCWE may induce infiltration of immune cells.

Massive CD11b positive cells infiltrate the lung tissues with ALI induced by LCWE

Based on the above analyses, Toll/NF-κB and TNF signaling pathways are turned on during ALI by both LCWE and LPS. The activation of these pathways results in the infiltration of many immune cells into the pathological loci. To understand the cells migrating to the ALI loci, we performed immune infiltration analysis using our RNA-seq data with the CIBERSORT algorithm (Fig. 4A). Among the immune cells, M1 macrophages and the activated CD4 memory T cells increased in the injured tissues in response to LCWE stimulation. To identify the types of immune cells migrating in response to inflammatory stimulation in injured lung tissues, we first stained the lung tissues with anti-IL-1β antibodies to confirm inflammation in ALI. After LPS or LCWE stimulation, IL-1β positive cells increased, indicating inflammation in ALI was induced by LPS or LCWE (Fig. 4B). To know further the migrating cell type in the injury tissues, we used antibodies against CD11b to identify macrophages, monocytes, and neutrophils (Fig. 4B). Both LPS and LCWE inductions increased CD11b positive cell infiltration in the injured lungs, albeit a few CD4 positive cells appeared in the injured lung induced by LCWE (Fig. 4B).

LCWE activates NF-κB and TNF signaling through TLR2, different from LPS through TLR4

Generally, monocytes patrol the bloodstream and migrate into the injured tissues in response to inflammatory stimuli. Eventually, the inflammatory monocytes differentiate into macrophages to help the host clear injured tissues and microbes[24–27]. Moreover, Toll-like receptors (TLRs) are important mediators of inflammatory pathways[24,26,28]. Hence, to understand how macrophages are activated and migrated to injured tissue, we knocked down TLR2 or TLR4 in THP-1 monocytes (THP-1) and induced the cells with LCWE or LPS (Fig. 5A, B). The results showed that TLR2 mRNA silencing significantly disrupted LCWE-induced, but did not affect LPS-induced, proinflammatory cytokines IL6 and TNFA expression, suggesting that TLR2 is a specific LCWE receptor to activate monocyte-mediated inflammation (Fig. 5A). In contrast, when TLR4 was silenced by shRNA (Fig. 5B), LPS-induced *IL6* and *TNFA* mRNA expressions were significantly and almost completely downregulated, while shTLR4 did not affect LCWE induction. It confirmed the well-known notion that TLR4 is the LPS receptor (Fig. 5B). The general proinflammatory cytokine IL1B expression in mRNA and protein levels was jointly regulated by TLR2 and TLR4 (Fig. 5A–C). Since these cytokines are the main factors amplifying inflammation in ALI, we concluded that LCWE induces ALI through TLR2, unlike LPS, which acts through TLR4.

MYD88 is the canonical adaptor of TLR-mediated signaling pathways[26]. To verify the essential role of MYD88 in LCWE-induced ALI, we knocked out MYD88 in THP-1 monocytes and induced cells with LPS or LCWE. The results showed that MYD88 ablation blocked LPS or LCWE-activated proinflammatory cytokine expression, including *IL6*, *TNFA*, and *IL1B* (Fig. 5D, E). Similarly, when we knocked down TNFR1 (Fig. 5F, G), both *IL6* and *IL1B* levels were significantly downregulated in response to LCWE or LPS stimulation, suggesting that TNFα is an amplifying factor of inflammatory signaling in ALI induced by LCWE or LPS.

NLRP3 inflammasome contributes to inflammation induced by LCWE

Overactive inflammation leads to the formation of inflammasomes[29–32]. To investigate whether the NLRP3 inflammasome is involved in LCWE-induced ALI, we knocked out the sensor protein NLRP3 with CRISPR-Cas9 lentivirus in THP-1 cells and induced cells with LCWE (Fig. 6A). Interestingly, quantitative PCR results indicated that the loss of NLRP3 significantly blocked the mRNA expression of *IL6*, *TNFA*, and *IL1B*

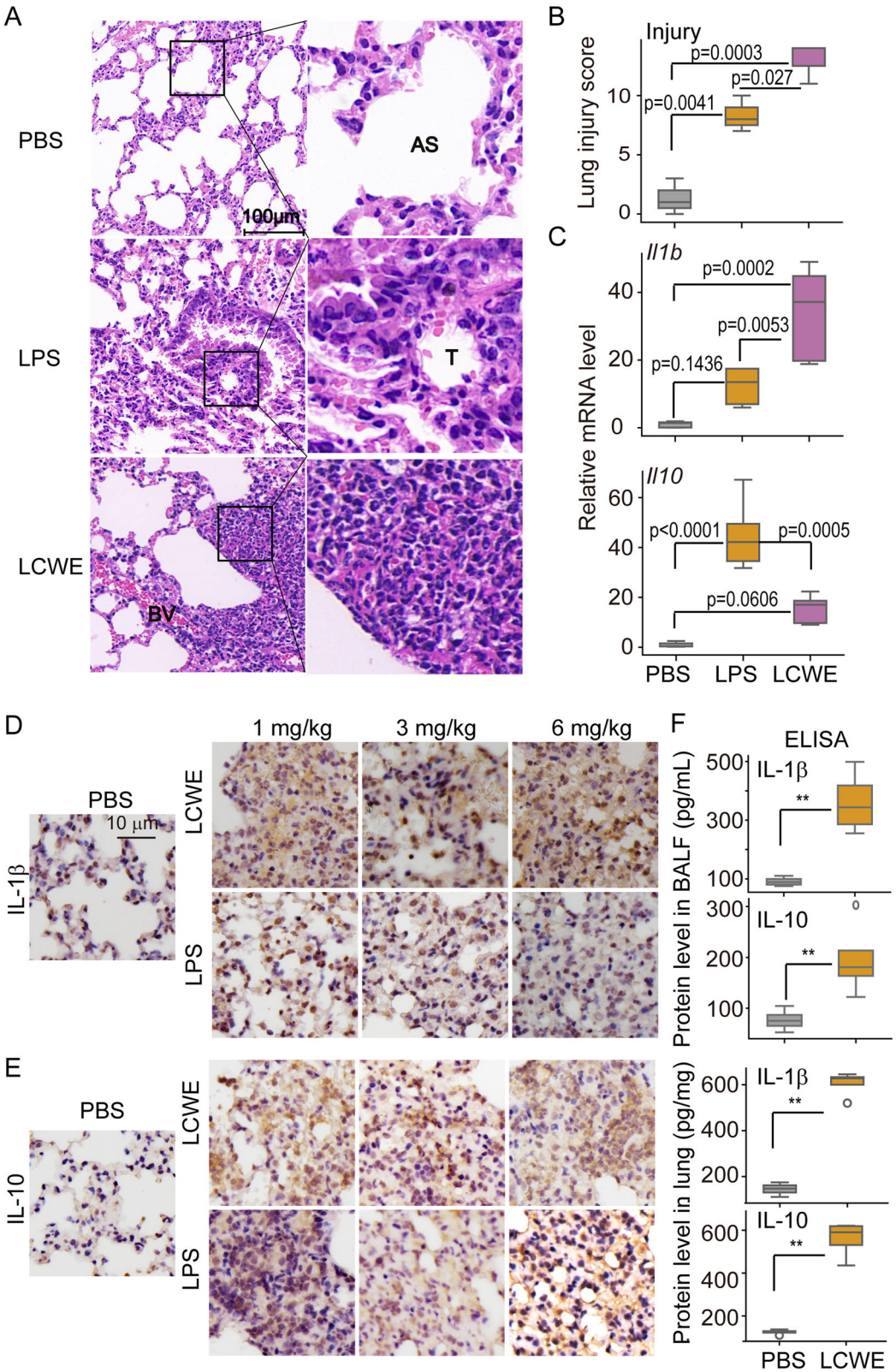

Fig. 1 | Establishment of LCWE-induced ALI murine model. A H&E staining of mouse lungs treated with PBS, 3 mg/kg of LPS or LCWE for 24 h. After treatment, animals were anesthetized with avertin, then lung tissues were collected after perfusion with formaldehyde. AS: Alveolus, BV: Blood Vessels, T: Trachea. **B** Pathological injury scores were collected in a blinded fashion by pathologists using H&E staining sections of mouse lung tissues after treatment with LPS or LCWE. Statistical analysis: One-way ANOVA test with *p*-value as indicated, $n = 5$. Error bar: SD. **C** *Il1b* and *Il10* mRNA levels of lung tissues induced with PBS, LPS, or LCWE by RT-qPCR. Statistical analysis: One-way ANOVA test with *p*-value as indicated, $n = 5$. Error bar: SD. **D**, **E** IL-1β and IL-10 immunostaining of lung tissues with ALI induced with 1, 3, 6 mg/kg of LPS or LCWE for 24 h. **F** IL-1β and IL-10 protein levels in both lung tissues and BALF were measured by ELISA. Statistical analysis T-test $^{**}p < 0.01$, $n = 4$. Error bar: SD.

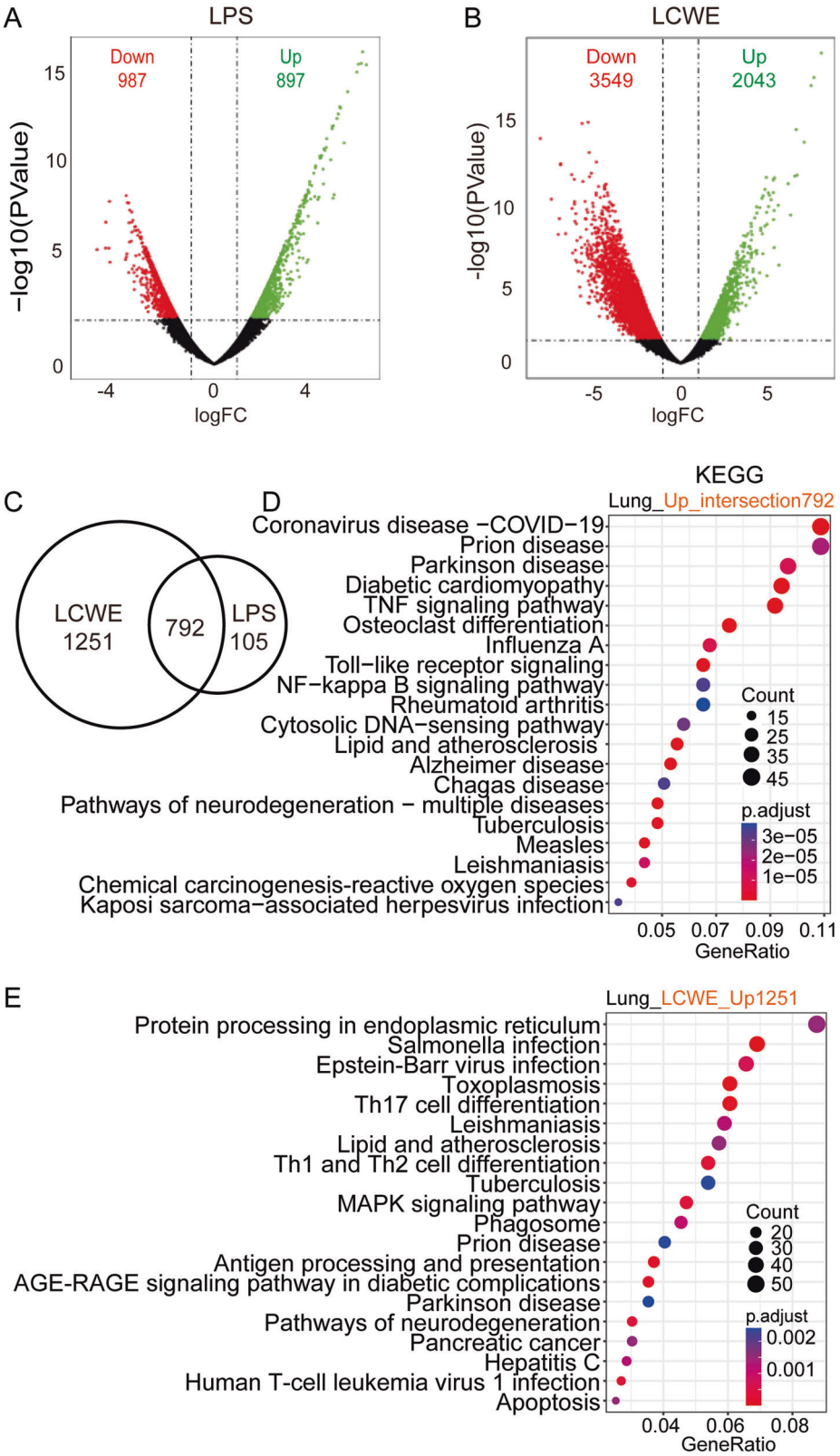

Fig. 2 | LCWE activates the inflammatory signaling pathways and promotes T-helper cell differentiation in ALI. A, **B** Volcano plots of the differentially regulated genes of the lungs by LPS (**A**) or LCWE (**B**), based on the data from RNA-seq analysis of the regulated genes in ALI induced by LPS or LCWE. **C** Similar to (**A**, **B**), Venn diagram plots of the upregulated genes in ALI induced by LPS and/or LCWE. **D**, **E** Similar to (**A**, **B**), KEGG analysis of the upregulated genes in ALI induced by LPS and LCWE (**D**), by LCWE only (**E**).

promoted by LCWE, similar to LPS. At the protein level, pro-IL-1β induction by LCWE or LPS was significantly disrupted by NLRP3 knockout (Fig. 6B). Both LCWE and LPS promoted IL-1β mRNA expressions in either THP-1 macrophages or primary BMDM, suggesting macrophages are of importance for LCWE-induced inflammation (Fig. S5A–D). We prepared BMDM cells from Wild-type (WT) or NLRP3 knockout (*Nlrp3*$^{-/-}$) mice and treated cells with LPS or LCWE. Similarly to those in THP-1 monocytes, in BMDM macrophages, the *Il6*, *Tnfa*, and *Il1b* mRNA expressions were significantly upregulated by LCWE or LPS, but blocked by *Nlrp3* genetically knocked out (Fig. 6C). Immunoblotting assays confirmed that pro-IL-1β was significantly increased by *Nlrp3* ablation in response to LCWE or LPS (Fig. 6D), suggesting processing of cleaved IL-1β was inhibited. We further wanted to know the Nlrp3 change in the mouse lungs treated with LCWE or LPS. Expectedly, Nlrp3 protein levels were significantly upregulated by

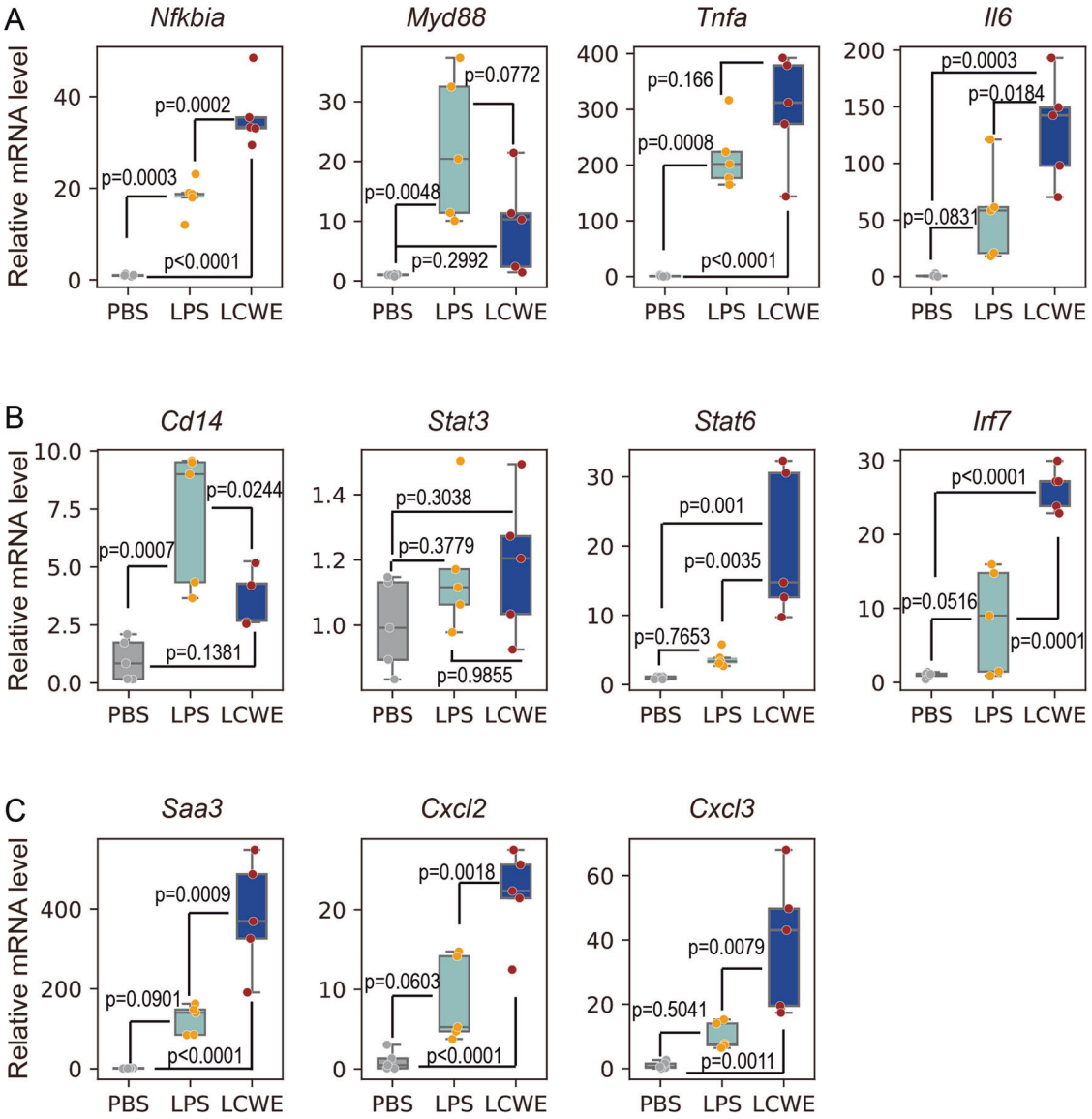

Fig. 3 | Genes in NF-κB and chemokine signaling pathways were activated by LCWE in ALI. A–C RT-qPCR validation of gene expression in NF-κB pathway (**A**), Jak/Stat pathway (**B**), and Chemokine signaling pathway (**C**) of ALI induced by LPS or LCWE. One-way ANOVA test with *p*-value indicated, $n = 5$. Error bar: SD.

LCWE, similar to LPS (Fig. 6E). Since Nlrp3 inflammasome activation leads to cleaved IL-1β release, we detected both pro-IL-1β and cleaved IL-1β changes. LCWE decreased the level of pro-IL-1β proteins and promoted the production of cleaved-IL-1β (Fig. 6F). However, when *Nlrp3* was knocked out, pro-IL-1β proteins increased but cleaved IL-1β proteins decreased in response to LCWE induction compared to wild-type animals (Fig. 6F). These data together showed that NLRP3 is an important mediator in the inflammation associated with ALI induced by LCWE.

Nlrp3 ablation disrupts inflammation and ALI induced by LCWE

To support the above hypothesis, we continued investigating the NLRP3 deletion effect on the downstream cytokines. We treated *Nlrp3*$^{-/-}$ mice with LCWE, using wild-type animals as controls. We found that the mRNA levels of *Il6*, *Tnfa*, and *Il1b* were all promoted in response to LCWE, and *Nlrp3* deletion significantly decreased them (Fig. 7A). Subsequently, we stained the lung tissues with anti-IL-1β and anti-IL-10, and repeatedly found that IL-1β and IL-10 increased upon LCWE stimulation. Importantly, *Nlrp3* loss disrupted IL-1β and IL-10 expression induced by LCWE, suggesting the promoted inflammation was blocked by *Nlrp3* deletion (Fig. 7B). To know Nlrp3 effects on cell migration to ALI tissues, we immunostained the mouse lungs with CD11b and CD14 antibodies. It showed that the migrated cells were mainly CD11b positive and partially CD14 positive. The infiltration of these immune cells in the lung was blocked by *Nlrp3* deletion.

Discussion

In this study, we successfully established a murine model of ALI induced with Gram-positive bacteria cell wall extract (Figs. 1, S1). As a technical control, 3 mg/kg of LPS was often used to induce ALI for the study of Gram-negative bacterial pneumonia. In our model, 1 to 6 mg/kg of LCWE induced most mice with comparable inflammation to LPS, and we chose 3 mg/kg of LCWE for the ALI model and 80% of mice appeared ALI. Following damage to lung parenchyma or vasculature, both ALI and ARDS have features of rapid respiratory failure[33]. Patients with ARDS often die from respiratory failure[34,35], and another challenge for the therapy of this severe disease ARDS is tissue heterogeneity[36]. Thus, better understanding of the cause and mechanism of subphenotypes of ARDS is essential for precision medicine[34]. Studies on ALI caused by Gram-positive bacteria will shed light on the target therapy of ARDS. Even though a couple of studies with Gram-positive bacteria-induced ALI have unveiled signaling pathways and key factors in the process, a lack of understanding of differentially regulated genes and a

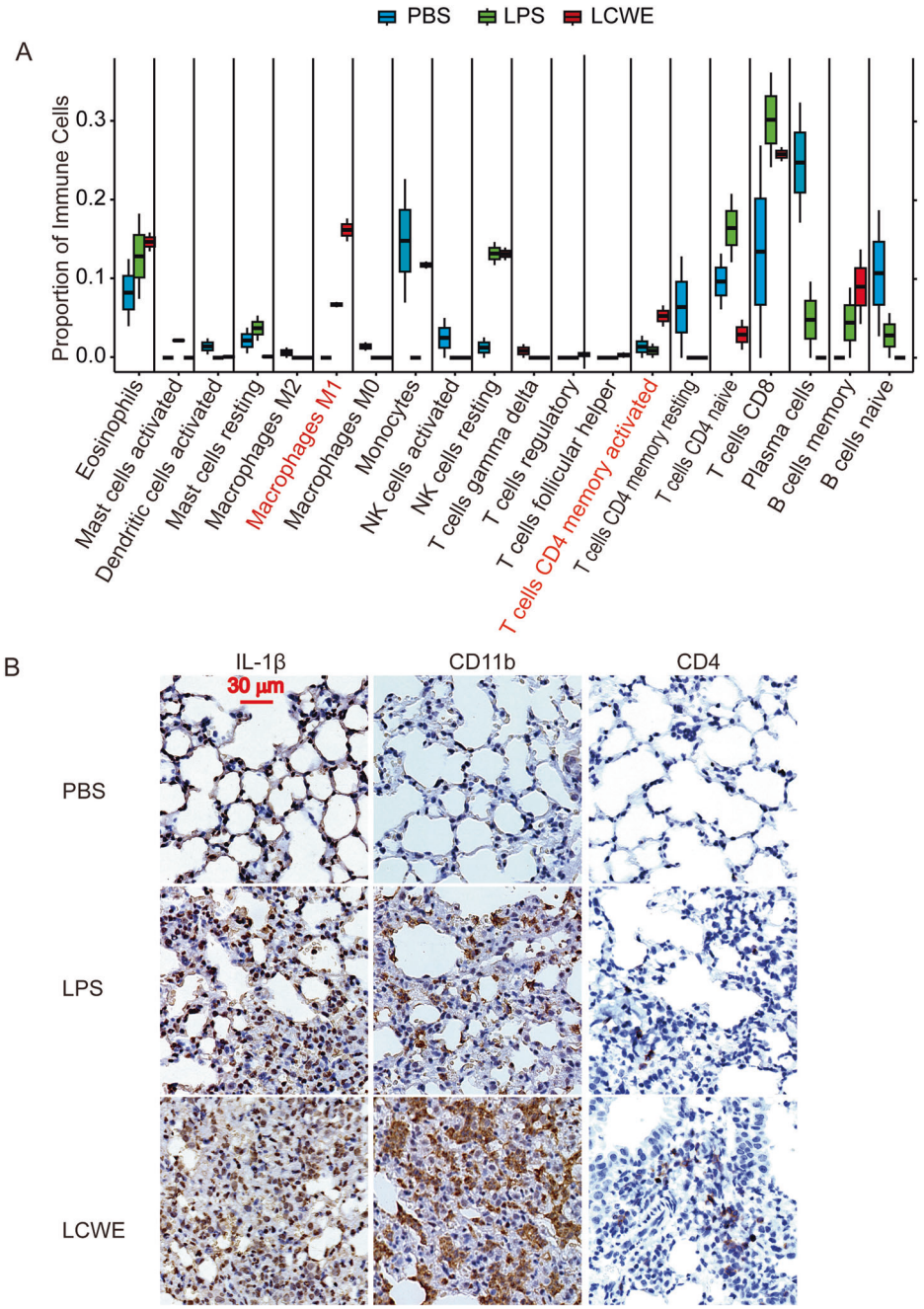

Fig. 4 | Immune infiltration analysis and staining suggested that immune cells migrate to lung tissues in either LPS- or LCWE-induced ALI. **A** Proportion of immune cells in ALI lung tissues treated with 3 mg/kg of LPS or LCWE, and the analysis was based on the differentially regulated genes from RNA-seq analysis. **B** IL-1β, CD11b, and CD4 levels were shown by DAB staining in the lung tissues with ALI induced by LPS or LCWE.

well-established model impedes the identification of new targets of ALI. In addition, the cell wall extracts of Gram-positive bacteria have not been used to establish a murine ALI model. Based on our knowledge, this is the first report of an experimental murine ALI model induced with gram-positive cell wall extract. Hence, our study is important for the clinic to find new therapy for ALI/ARDS.

Using the established LCWE-induced ALI model, our transcriptomic analyses highlighted that signaling pathways of Toll-like receptor, NF-κB, and TNF are significantly activated in LCWE-induced ALI (Figs. 2, S2). Expression levels of the key genes which include *Nfkbia*, *Tnfa*, *Il6*, and *CD14* in these pathways were verified by quantitative PCR (Fig. 3). As a result, lung cells develop inflammation and immunity to clear pathogens and protect themselves from damage[37]. Mice with stimulation of LCWE have focal coronary arteritis, and TLR2 ablation reduces severe symptoms in Kawasaki disease[38]. In monocytes, we showed that LCWE triggers inflammatory signaling through TLR2, different from that LPS depends on TLR4. Subsequently, the activated signaling pathways converge to MYD88. These results were consistent with previous reports in macrophages[38]. In addition, we found that the down-regulation of the TLR receptor (TNFR1) impaired inflammatory cytokine expression (Fig. 5F, G), indicating the amplification role of TNF signaling in the inflammatory process in ALI. Hence, our detailed studies will provide insights for ALI induced by Gram-positive and negative bacteria components.

The key regulator in ALI induced by Gram-positive bacteria has been kept debate. In the study, using our well-established LCWE-induced cell model, we indicated that NLRP3 promotes LCWE-induced inflammation in monocytes, macrophages, and mouse lung and it is the essential regulator in LCWE-induced inflammation (Figs. 6 and 7). Strong inflammation in lung parenchyma and immune cells develops cytokine storm syndrome, which is mediated by inflammasomes and accompanied by cell death[22,39,40]. Inflammasomes are protein complexes activated by endogenous and exogenous pathogen stimuli[41], and the NLRP3 inflammasome is formed upon LPS

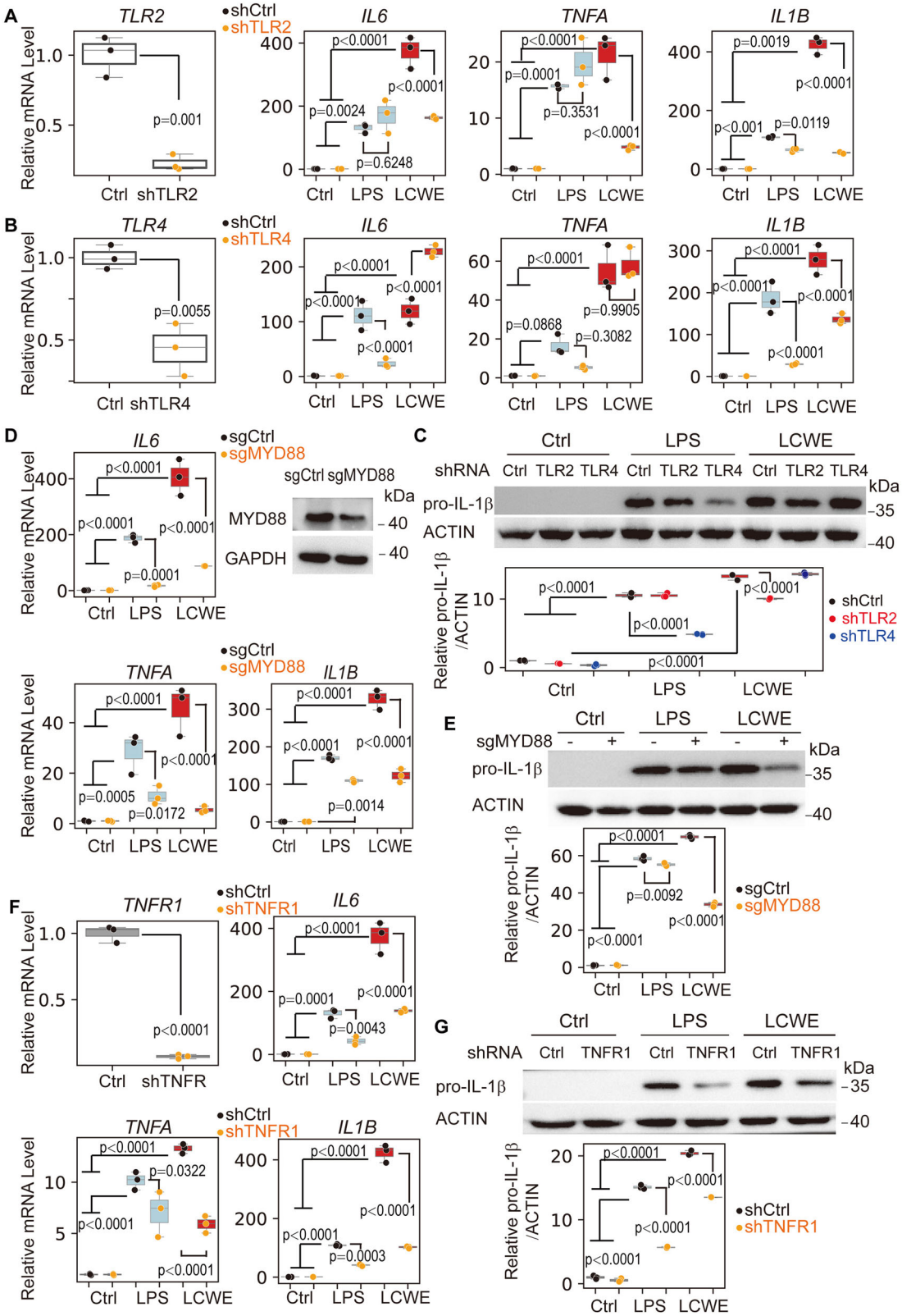

Fig. 5 | LCWE and LPS induce inflammation in THP-1 monocytes through TLR2 and TLR4, respectively. **A**–**C** The changes in the mRNA level of *IL6*, *TNFA*, and *IL1B* by RT-qPCR (**A**, **B**) and the changes of pro-IL-1β protein level by Immunoblotting (**C**) in human THP-1 monocytes in response to LPS or LCWE after knocking down TLR2 or TLR4. Statistical analysis: two-way ANOVA test with *p*-value as indicated. Error bar: SD. **D**–**G** After knocking out MYD88 (**D**, **E**) or TNFR1 (**F**, **G**), the pro-IL-1β protein level by Immunoblotting and the mRNA level changes of *IL6*, *TNFA*, and *IL1B* by RT-qPCR in THP-1 monocytes in response to LPS or LCWE stimulation. LPS:100 ng/mL, LCWE: 500 ng/mL. Statistical analysis: two-way ANOVA test with *p*-value as indicated. Error bar: SD.

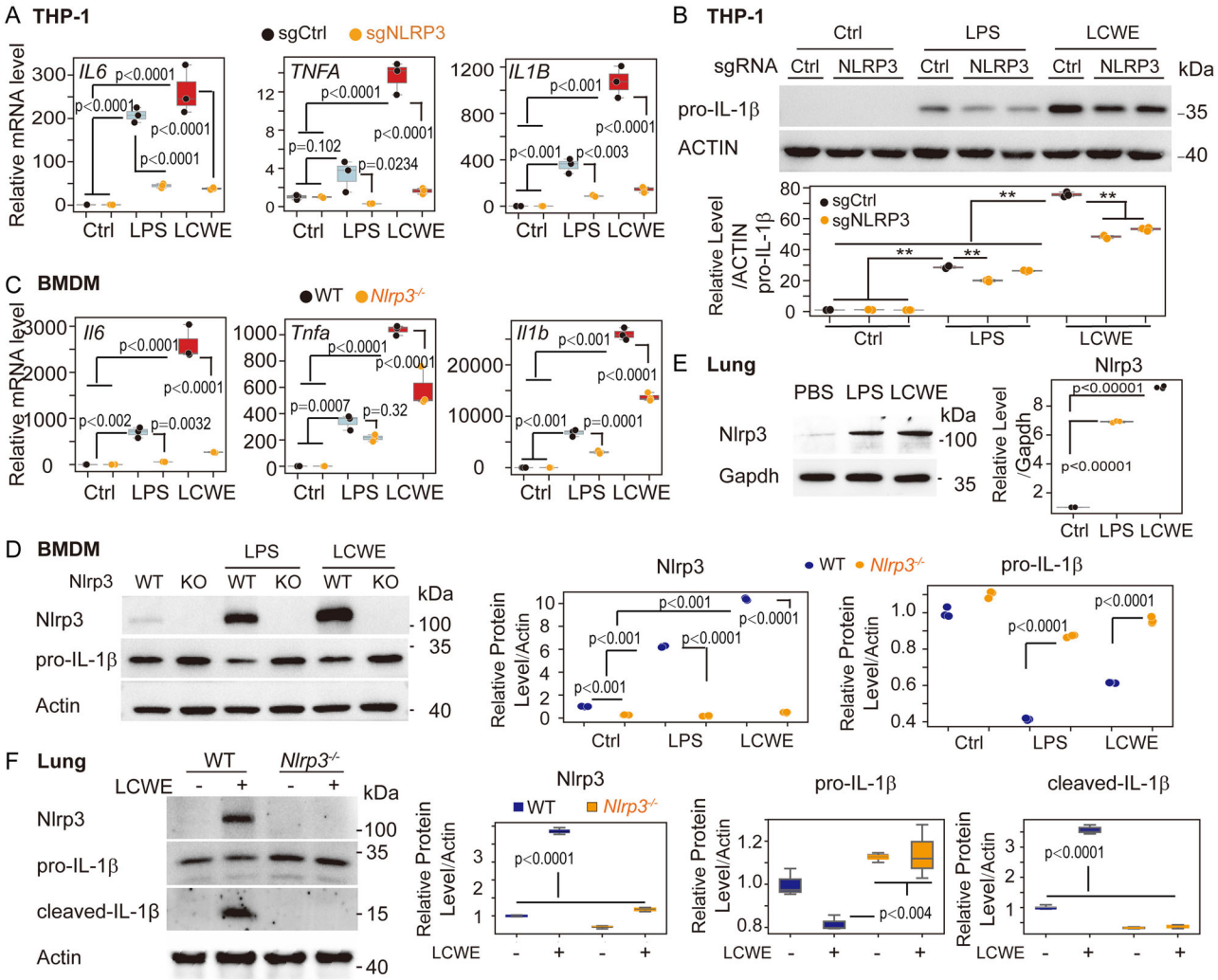

Fig. 6 | NLRP3 ablation disrupted the expression of inflammatory genes and the process of cleaved IL-1β in THP-1 monocytes and damaged lungs with ALI in response to LPS or LCWE. A, **B** After NLRP3 ablation in the human THP-1 monocyte cell line, the mRNA levels of *IL6*, *TNFA*, and *IL1B* (**A**) and the protein levels of pro-IL-1β (**B**) in response to LPS and LCWE were measured with qPCR and WB. Statistical analysis: two-way ANOVA test with *p*-value as indicated. Error bar: SD. **C**, **D** After Nlrp3 knockout in the mouse primary BMDMs, the mRNA levels of *IL6*, *TNFA*, and *IL1B* (**C**), and the protein levels of pro-IL-1β (**D**) were measured. Statistical analysis: two-way ANOVA test with *p*-value as indicated. Error bar: SD. **E** The protein level changes of Nlrp3 induced by LPS or LCWE in the mouse pooled ALI lung samples ($n = 5$) were analyzed by immunoblotting. One-way ANOVA test with *p*-value as indicated. Error bar: SD. **F** Before or after Nlrp3 knockout, the protein level changes of Nlrp3 and the pro- and cleaved- IL-1β levels induced by LCWE in the mouse pooled ALI lungs samples ($n = 5$) were analyzed by immunoblotting. Statistical analysis: two-way ANOVA test with p-value as indicated. Error bar: SD.

stimulation in ALI[21,42]. Hence, targeting NLRP3 inflammasome is an essential way to avoid damage from ALI induced by LPS[39]. However, due to the complexity of causes for the formation of NLRP3 inflammasome, more knowledge of the role of NLRP3 inflammasome in LCWE-induced ALI is very important to identify new therapy targets. In the mouse lung with ALI, the elevation of Nlrp3 and cleaved-IL-1β upon LCWE was disrupted by *Nlrp3* deletion (Fig. 6E, F), indicating that pyroptosis is possibly induced by LCWE and inhibited by loss of function of NLRP3 inflammasome.

Our data suggested that targeting Nlrp3 reduces LCWE-induced ALI, possibly by reduction of cytokines IL-6, TNFα, and IL-1β (Fig. 7A). It is known that these cytokines account for the immune microenvironment in injured tissues[43], attracting most leukocytes to the inflammatory loci[44]. As shown by CD11b and CD14, both neutrophils and monocytes/macrophages infiltrated to the injured lungs induced by LCWE but decreased after Nlrp3 loss of function (Fig. 7B). In addition, NF-κB p-p65 was downregulated when *Nlrp3* was deleted in response to LCWE stimulation (Figs. 7C, S6), suggesting that amplification of NF-κB signaling was regulated by Nlrp3 inflammasome in LCWE-induced ALI. The decrease of cleaved-IL-1β indicated that pyroptosis in injured lung cells was constrained by the loss of *Nlrp3* upon LCWE stimulation (Figs. 7C, S6). Hence, our study highlighted the possibility of targeting the process of mature IL-1β, and pyroptosis is a potential strategy to prevent Gram-positive bacteria-induced lung damage.

Taken together, using the cell wall extracts of Gram-positive bacteria, we established an LCWE-induced ALI murine model (Fig. 8). Unlike LPS, which depends on TLR4, LCWE-induced ALI depends on TLR2. Both LCWE and LPS depend on Myd88 to activate NF-κB signaling pathways and to induce the expression of cytokines such as IL6, TNFα, and IL-1β. These cytokines amplify NF-κB signaling and the NLRP3 inflammasome, attracting immune cells to the injured tissues and accounting for ALI and cell death. Hence, targeting NLRP3 could be an efficient approach for the treatment of ALI and ARDS induced by cell wall extracts of Gram-positive bacteria.

Methods

Ethics approval

This study was approved by the Biomedical Ethics and Animal Committee at the Anhui Medical University (LLSC20241345). We have complied with all relevant ethical regulations for animal use.

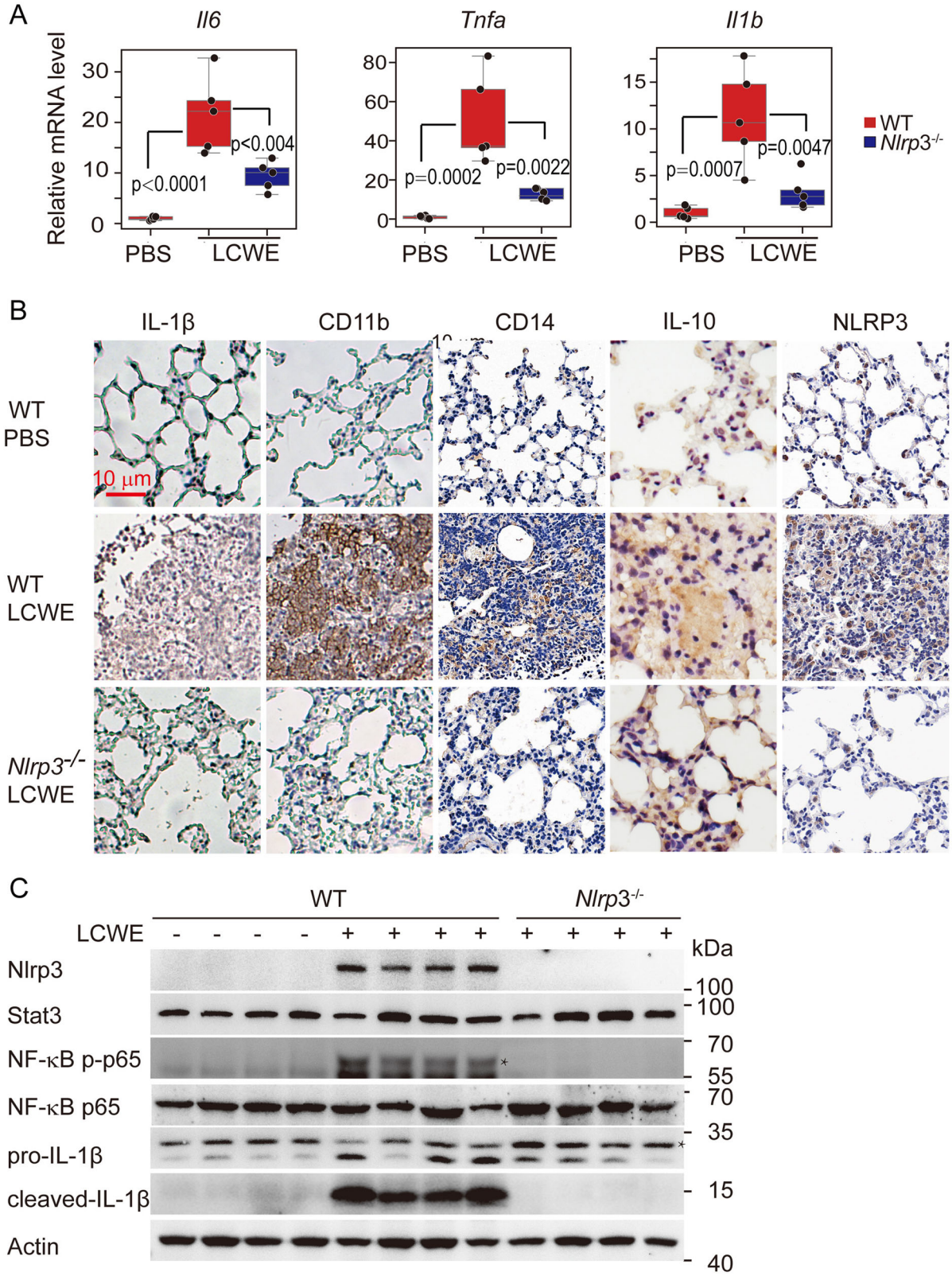

Fig. 7 | The Nlrp3 deletion blocked inflammation, and macrophage infiltration in ALI induced by LCWE. A The WT or *Nlrp3*$^{-/-}$ mice lungs were treated with LCWE at 3 mg/kg, the mRNA levels of *Il6*, *Tnfa*, and *Il1b* were measured by RT-qPCR ($n = 5$). Statistical analysis: two-way ANOVA test with *p*-value as indicated. Error bar: SD. **B** The above mouse lungs were stained with the specific antibodies against IL-1β, CD11b, CD14, IL-10, and NLRP3. **C** The WB results of Nlrp3, Stat3, NF-κB p-p65, NF-κB p65, pro-IL-1β, cleaved-IL-1β in WT or *Nlrp3*$^{-/-}$ mice treated with LCWE. * indicates the specific band.

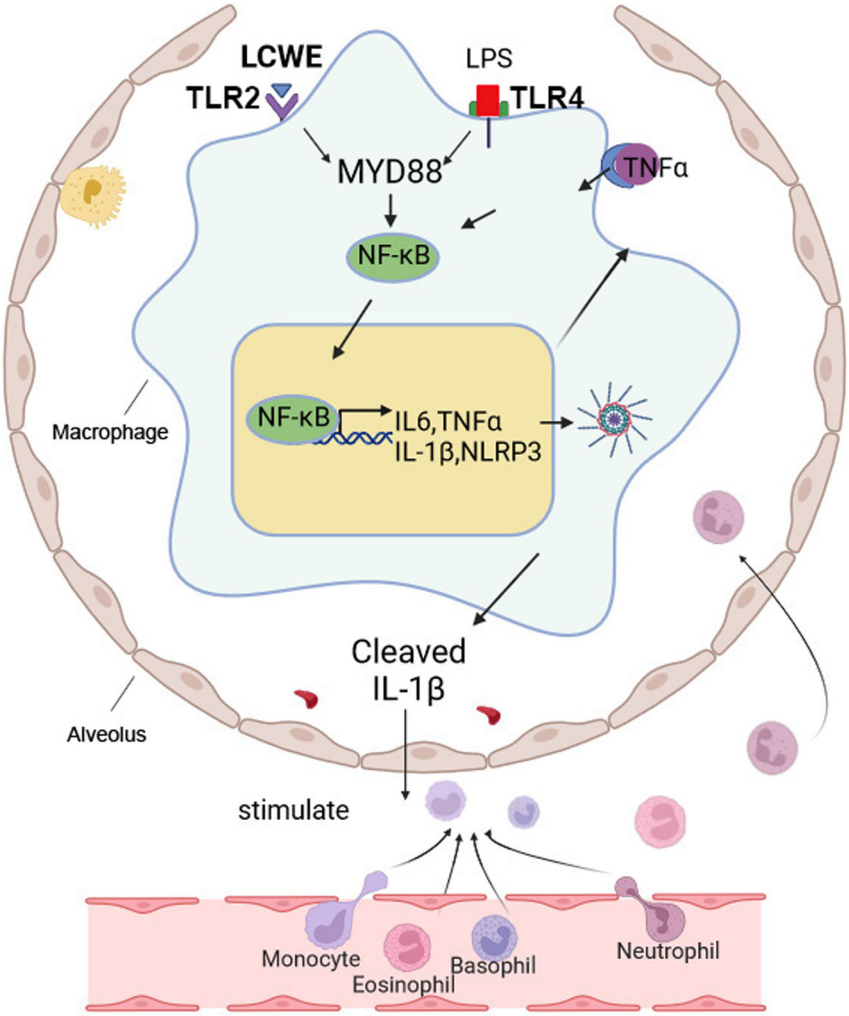

Fig. 8 | Model of LCWE-induced ALI. In macrophage cells, LCWE activates inflammatory signaling pathways through TLR2, unlike LPS through TLR4. MYD88 functions as the adaptor for the TLR receptors of both LCWE and LPS, activating the NF-κB signaling pathway and the expression of inflammatory cytokines including IL6, TNFα, pro-IL-1β, and NLRP3. These cytokines further increase inflammatory signaling, resulting in an inflammatory storm and ALI.

Cell culture and antibodies

THP-1 cells were cultured in RPMI 1640 media containing 10% FBS, 1% penicillin/streptomycin, and 1% L-glutamine. THP-1 macrophages were obtained from the induced THP-1 with 100 ng/mL of PMA (Abmole, #M4647). On day 0, BMDMs were prepared from the femur and tibia of C57BL/6 mice and were cultured in DMEM medium with 30% L929 conditioned media and 10% FBS (Complete Conditioned Medium) as described[45]. On day 3, the media was gently replaced with fresh Complete Conditioned Medium. After another 3 days (day 6), BMDMs were fully differentiated, and reseeded into six-well plates with standard DMEM medium for treatments. For induction, BMDM cells and THP-1 macrophages were treated with 100 ng/mL of LPS or 500 ng/mL of LCWE for 24 hours. Anti-CD11b (#GB11058, DAB, 1:600), anti-GAPDH (#AC22027016, 1:1000), and anti-Actin (#AC220730003, 1:1000) are from Servicebio. Anti-CD14 (#60253-1-Ig, DAB, 1:400) and anti-hIL-1β (#66737, DAB, 1:400) are from Proteintech. The antibodies from other suppliers include anti-CD4 (Abcam, #ab183685, DAB, 1:1000), anti-NLRP3 (Cell Signaling, #15101, WB, 1:1000), anti-NF-kB p65 (Cell Signaling, #8242, WB,1:1000), anti-NF-kB p-p65 (Santa Cruz, #sc-136548, WB, 1:1000) anti-NLRP3 (Servicebio, #GB114320, DAB, 1:300), anti-MYD88 (Wanleibio, #WL02494, 1:1000), anti-cleaved IL-1β (Affinity, #AF4006, WB, 1:1000) and anti-IL-10 (HUABIO, #ER65464, DAB, 1:200).

Mouse and ALI model

The C57BL/6 wild-type and *Nlrp3*$^{-/-}$ mice were maintained in the animal center at the Anhui Medical University. To establish the mouse model of acute lung injury (ALI), LPS (Sigma, #L2880) or LCWE (Prepared in the study) was administered into the lungs of 6-week-old male mice from the trachea at 1, 3, and 6 mg/kg after the mice were anesthetized with pentobarbital sodium at a dose of 3 mg/kg. After 24 h, the mice were sacrificed, and bronchoalveolar lavage fluid (BALF) and lung tissues were collected for RT-qPCR, immunoblotting, and ELISA assays. For tissue preparation of immunostaining, the mice were anesthetized with avertin and followed by perfusion. In detail, the thoraxes were opened, and the right auricle was cut. A perfusion needle was inserted into the left ventricle from the apex of the heart, and precooled PBS was injected until the liver turned pale.

Lung injury scoring

Lung injury was assessed according to the pathological manifestation of each section, including four items: the thickness of the alveolar wall, lung edema, neutrophil infiltration, and hemorrhage. Three pathologists blindly scored each item in six random fields with scores ranging from 0 to 4: normal (0), mild (1), moderate (2), moderate severe (3), and severe (4). The lung injury score of each sample is the sum of the average scores of each item.

ELISA

Lung tissue was minced in ELISA lysate buffer. After centrifugation of 8000 × *g* at 4 °C for 5 min, the supernatant was collected for assay, and the protein concentration of the supernatant was measured by BCA assay. 200 μL of BALF was applied directly for assay. The concentrations of IL-1β (IL-1β ELISA kit: #KE10003, Proteintech) and IL-10 (IL-10 ELISA kit: #KE10103, Proteintech) were determined according to the manufacturer's instructions.

Lactobacillus casei culture and preparation of LCWE

Lactobacillus casei (ATCC11578) was purchased from Xinyang Zhongjian Metrology Biotechnology, China, and was cultured in MRS media, which were prepared at 1:1 (V/V) with the Part A and B media and autoclaved separately. Part A included glucose (20 g/L) and magnesium sulfate heptahydrate (0.58 g/L). Part B contained peptone (10 g/L), beef extract (10 g/L), yeast extract (5 g/L), dipotassium hydrogen phosphate (1.5 g/L), Tween-80 (1 mL/L), diammonium citrate (2 g/L), sodium acetate (3 g/L), and manganese sulfate monohydrate (0.25 g/L). The pH was adjusted to 6.2–6.6. LCWE was prepared as described with minor modifications[46]. In detail, the bacterial cells were incubated in the MRS media without shaking for 48 h at 37 °C and were collected at 10,000 × *g* for 10 minutes at 4 °C. The bacterial pellet was suspended in PBS (twice of the packed cell volume) and 4% SDS (4 times of the packed cell volume) sequentially and kept at room temperature for 18 h. Subsequently, it was thoroughly washed 8 times with PBS through centrifugation to eliminate SDS, confirmed by the absence of precipitation with 2 M KCl. The PBS-washed pellet was sequentially incubated with 250 μg/mL of RNase A, DNase A, and Trypsin (SparkJade). The resulting cell wall preparation was extensively washed with PBS and sonicated for 2 h at the concentration of 0.25 g of wet pellet/mL PBS at maximum power. The resulting cell wall fragments were spun at 12,000 rpm for 20 min to collect the supernatant followed by centrifugation at 40,000 × *g* for 1 h at 4 °C. The concentration of carbohydrates in the cell wall extract was determined using the Phenol Sulfuric Acid method[46].

Immunohistology and immunoblotting

Hematoxylin & Eosin staining and immunostaining were performed on the paraffin sections of lung tissues as previously described[47]. For immunoblotting, the dounced tissues or the cultured cells were washed with ice-cold PBS for three times. Subsequently, the samples were lysed on ice with RIPA buffer (50 mM Tris pH 8.0, 150 mM NaCl, 0.05% SDS, 0.5% DOC, 1% NP-40) supplemented with protease inhibitors (Abmole). The protein concentration was determined using a BCA assay (Vazyme). The protein lysates were loaded on SDS-PAGE and transferred to the nitrocellulose membrane (Merck, #IPVH00010). The blot was blocked with 5% non-fat milk in TBST and incubated with the primary antibodies in 2% BSA in TBST overnight at 4 °C. After incubation with the HRP-linked secondary antibodies (Abbart) for 1 h at room temperature, the bands were detected with ECL and scanned with a SHST ChemiDoc Imager (Shenhua, China).

pLKO-shRNA and CRISPR-Cas9 vectors, lentivirus preparation and infection

pLKO.1 from Addgene was used for shRNA knockdown. LentiCRISPR-V2 was used for RNA-guide gene editing. For lentivirus packaging, the pLKO.1 or LentiCRISPR-V2 plasmids with targeting sequences, together with the package plasmids of VSV-g and Δ8.9 were transfected into 293T cells using PEI (Yeasen, #40816ES02/03). Lentiviruses were collected after transfection for 48 and 72 h. For infection, THP-1 cells were cultured with 50% virus (original virus: fresh media = 1:1) and 8 μg/ml of polybrene.

RT-PCR and qPCR

Total RNA was extracted using TRIzol (Ambion, #400008). The RNA concentration was measured using SH-NanoOne (Shenhua, China). cDNA was synthesized using MonScript RTIII All-in-One Mix with dsDNase (Monad, #MR05101). Quantitative PCR was performed using MonAmp qPCR Mix reagent (Monad, #00007547-130712) with a LightCycle real-time PCR system (Roche). GAPDH was used for normalization.

RNA-seq and bioinformatics analysis

RNA-seq and bioinformatics analysis were performed at the Sequencing and Bioinformatics Center at the Anhui Medical University. In detail, mRNA was isolated using Oligo-dT magnetic beads (Vazyme, #N401) from the total RNA. cDNA was synthesized using SuperScript II (Invitrogen, #18064014). The cDNA library was prepared using Tn5 DNA Library Prep Kit (Transgen, #KP101-11). The cDNA library was applied for PE150 sequencing. The quality of Fastq data was controlled by Fastqc and analyzed using the RNA-seq pipeline[48]. The relative expression levels were determined with featureCounts[49], and the differentially regulated genes were called by DEseq2 program in the pipeline with fold-change >2 and padj < 0.05. Bioinformatics analyses including GO, KEGG, and CIBERSORT were analyzed using R studio.

Statistical and reproducibility

Statistical analysis was performed using the two-tailed unpaired Student's t-test provided by Microsoft Excel and one-way or two-way ANOVA test combined with Tukey's HSD test in Python (Spyder IDE). A P value of <0.05 was considered significant. All experiments were performed at least three times independently to ensure reproducibility, with consistent results observed across replicates. For experiments lacking statistical analysis, reproducibility was assessed by repeating the experiments under the same conditions to confirm consistency in outcomes.

Data availability

All data generated or analyzed during this study are included in this published article and its supplementary information files. Source data can be found in Supplementary Data 1. The datasets generated during the current study have also been deposited in the NCBI GEO repository under the accession number GSE273921.

Received: 23 July 2024; Accepted: 3 January 2025;
Published online: 07 January 2025

References

1. Jain, S. et al. Community-acquired pneumonia requiring hospitalization among U.S. adults. *N. Engl. J. Med.* **373**, 415–427 (2015).
2. Long, M. E., Mallampalli, R. K. & Horowitz, J. C. Pathogenesis of pneumonia and acute lung injury. *Clin. Sci.* **136**, 747–769 (2022).
3. Aliberti, S., Dela Cruz, C. S., Amati, F., Sotgiu, G. & Restrepo, M. I. Community-acquired pneumonia. *Lancet* **398**, 906–919 (2021).
4. Lee, C. H. et al. Using a targeted metabolomics approach to explore differences in ARDS associated with COVID-19 compared to ARDS caused by H1N1 influenza and bacterial pneumonia. *Crit. Care* **28**, 63 (2024).
5. Asif, H. et al. Mycobacterium abscessus—bronchial epithelial cells cross-talk through type I interferon signaling. *Am. J. Resp. Crit. Care* **201**, 2888 (2020).
6. Xu, Z. L. et al. Candida albicans-induced acute lung injury through activating several inflammatory signaling pathways in mice. *Int Immunopharmacol.* **72**, 275–283 (2019).
7. Falsey, A. R. et al. Bacterial complications of respiratory tract viral illness: a comprehensive evaluation. *J. Infect. Dis.* **208**, 432–441 (2013).
8. McCullers, J. A. Do specific virus-bacteria pairings drive clinical outcomes of pneumonia? *Clin. Microbiol Infec.* **19**, 113–118 (2013).
9. Ahn, D. S. et al. Secretion of IL-16 through TNFR1 and calpain-caspase signaling contributes to MRSA pneumonia. *Mucosal Immunol.* **7**, 1366–1374 (2014).
10. Girardin, S. E. et al. Nod2 is a general sensor of peptidoglycan through muramyl dipeptide (MDP) detection. *J. Biol. Chem.* **278**, 8869–8872 (2003).
11. Kapetanovic, R. et al. Contribution of NOD2 to lung inflammation during Staphylococcus aureus-induced pneumonia. *Microbes Infect.* **12**, 759–767 (2010).
12. Kebaier, C. et al. Staphylococcus aureus α-hemolysin mediates virulence in a murine model of severe pneumonia through activation of the NLRP3 inflammasome. *J. Infect. Dis.* **205**, 807–817 (2012).
13. Paudel, S. et al. NLRC4 suppresses IL-17A-mediated neutrophil-dependent host defense through upregulation of IL-18 and induction

of necroptosis during Gram-positive pneumonia. *Mucosal Immunol.* **12**, 247–257 (2019).
14. Johnson, E. R. & Matthay, M. A. Acute lung injury: epidemiology, pathogenesis, and treatment. *J. Aerosol Med. Pulm. D.* **23**, 243–252 (2010).
15. Matthay, M. A. & Howard, J. P. Progress in modelling acute lung injury in a pre-clinical mouse model. *Eur. Respir. J.* **39**, 1062–1063 (2012).
16. Lv, X. J., Lu, X. M., Zhu, J. P. & Wang, Q. Lipopolysaccharide-induced acute lung injury is associated with increased ran-binding protein in microtubule-organizing center (RanBPM) molecule expression and mitochondria-mediated apoptosis signaling pathway in a mouse model. *Med. Sci. Monit.* **26**, e923172 (2020).
17. Tsikis, S. T. et al. Lipopolysaccharide-induced murine lung injury results in long-term pulmonary changes and downregulation of angiogenic pathways. *Sci. Rep.* **12**, 10245 (2022).
18. Novak, J. et al. New insights into the pathogenesis of IgA nephropathy. *Kidney Dis.* **1**, 8–18 (2015).
19. Bhattacharya, J. & Matthay, M. A. Regulation and repair of the alveolar-capillary barrier in acute lung injury. *Annu. Rev. Physiol.* **75**, 593–615 (2013).
20. Matthay, M. A., Ware, L. B. & Zimmerman, G. A. The acute respiratory distress syndrome. *J. Clin. Invest* **122**, 2731–2740 (2012).
21. Rathinam, V. A. K., Zhao, Y. & Shao, F. Innate immunity to intracellular LPS. *Nat. Immunol.* **20**, 527–533 (2019).
22. Dolinay, T. et al. Inflammasome-regulated cytokines are critical mediators of acute lung injury. *Am. J. Resp. Crit. Care* **185**, 1225–1234 (2012).
23. LeVan, T. D. et al. A common single nucleotide polymorphism in the CD14 promoter decreases the affinity of Sp protein binding and enhances transcriptional activity. *J. Immunol.* **167**, 5838–5844 (2001).
24. Nova, Z., Skovierova, H. & Calkovska, A. Alveolar-capillary membrane-related pulmonary cells as a target in endotoxin-induced acute lung injury. *Int. J. Mol. Sci.* **20**, 831 (2019).
25. Lee, J. W. Macrophage-derived microvesicles' pathogenic role in acute lung injury. *Thorax* **71**, 975–976 (2016).
26. Jiang, Y. L. et al. Single cell RNA sequencing identifies an early monocyte gene signature in acute respiratory distress syndrome. *JCI insight* **5**, e135678 (2020).
27. Lee, J. W. et al. The role of macrophages in the development of acute and chronic inflammatory lung diseases. *Cells* **10**, 897 (2021).
28. Root-Bernstein, R. Innate receptor activation patterns involving TLR and NLR synergisms in COVID-19, ALI/ARDS and sepsis cytokine storms: a review and model making novel predictions and therapeutic suggestions. *Int. J. Mol. Sci.* **22**, 2108 (2021).
29. Li, Y. X. et al. Inflammasomes as therapeutic targets in human diseases. *Signal Transduct. Tar.* **6**, 247 (2021).
30. Yao, J., Sterling, K., Wang, Z., Zhang, Y. & Song, W. H. The role of inflammasomes in human diseases and their potential as therapeutic targets. *Signal Transduct. Tar.* **9**, 10 (2024).
31. McVey, M. J., Steinberg, B. E. & Goldenberg, N. M. Inflammasome activation in acute lung injury. *Am. J. Physiol. -Lung C.* **320**, L165–L178 (2021).
32. Jones, H. D. et al. The NLRP3 inflammasome is required for the development of hypoxemia in LPS/mechanical ventilation acute lung injury. *Am. J. Respir. Cell Mol. Biol.* **50**, 270–280 (2014).
33. Raghavendran, K. & Napolitano, L. M. ALI and ARDS: challenges and advances preface. *Crit. Care Clin.* **27**, Xiii–Xiv (2011).
34. Thompson, B. T., Chambers, R. C. & Liu, K. D. Acute respiratory distress syndrome. *N. Engl. J. Med.* **377**, 562–572 (2017).
35. Ramji, H. F., Hafiz, M., Altaq, H. H., Hussain, S. T. & Chaudry, F. Acute respiratory distress syndrome; a review of recent updates and a glance into the future. *Diagnostics* **13**, 1528 (2023).
36. Wenzel, S. E. Asthma phenotypes: the evolution from clinical to molecular approaches. *Nat. Med.* **18**, 716–725 (2012).
37. Islam, M. N. et al. The mitochondrial calcium uniporter of pulmonary type 2 cells determines severity of acute lung injury. *Nat. Commun.* **13**, 5837 (2022).
38. Rosenkranz, M. E. et al. TLR2 and MyD88 contribute to extract-induced focal coronary arteritis in a mouse model of Kawasaki disease. *Circulation* **112**, 2966–2973 (2005).
39. Zheng, D. P., Liwinski, T. & Elinav, E. Inflammasome activation and regulation: toward a better understanding of complex mechanisms. *Cell Discov.* **6**, 36 (2020).
40. Fan, E. K. Y. & Fan, J. Regulation of alveolar macrophage death in acute lung inflammation. *Resp. Res.* **19**, 50 (2018). ARTN.
41. Schroder, K. & Tschopp, J. The inflammasomes. *Cell* **140**, 821–832 (2010).
42. Grailer, J. J. et al. Critical role for the NLRP3 inflammasome during acute lung injury. *J. Immunol.* **192**, 5974–5983 (2014).
43. Manicone, A. M. Role of the pulmonary epithelium and inflammatory signals in acute lung injury. *Expert Rev. Clin. Immunol.* **5**, 63–75 (2009).
44. Ling, D. et al. Identification of immune infiltration and effective immune biomarkers in acute lung injury by bioinformatics analysis. *Cell Transplant.* https://doi.org/10.1177/09636897221124485 (2022).
45. Assouvie, A., Daley-Bauer, L. P. & Rousselet, G. in *Macrophages: Methods and Protocols* (ed. Rousselet, G.) 29–33 (Springer New York, 2018).
46. Lehman, T. J., Allen, J. B., Plotz, P. H. & Wilder, R. L. Polyarthritis in rats following the systemic injection of *Lactobacillus casei* cell walls in aqueous suspension. *Arthritis Rheum.* **26**, 1259–1265 (1983).
47. Thompson, E. M. et al. Prognostic value of medulloblastoma extent of resection after accounting for molecular subgroup: a retrospective integrated clinical and molecular analysis. *Lancet Oncol.* **17**, 484–495 (2016).
48. Pertea, M., Kim, D., Pertea, G. M., Leek, J. T. & Salzberg, S. L. Transcript-level expression analysis of RNA-seq experiments with HISAT, StringTie and Ballgown. *Nat. Protoc.* **11**, 1650–1667 (2016).
49. Liao, Y., Smyth, G. K. & Shi, W. featureCounts: an efficient general purpose program for assigning sequence reads to genomic features. *Bioinformatics* **30**, 923–930 (2014).

Acknowledgements

This study was supported by grants from the National Natural Science Foundation of China (82073124, 32270799).

Author contributions

X.S., S.L., and L.Z. designed the work and analyzed the results. X.S. and S.L. wrote the manuscript with help from all authors. L.G., J.Z., and Q.N. conceived and carried out most of the experiments. B.X., S.X., A.Z., Q.S, Q.L., S.L., Y.L., and W.S. did part of the experiments. Z.Z. established the LPS-induced ALI mouse model. All authors reviewed the manuscript.

Competing interests

The authors declare no competing interests.

Additional information

Supplementary information The online version contains supplementary material available at https://doi.org/10.1038/s42003-025-07462-9.

Correspondence and requests for materials should be addressed to Lei Zhao, Shuzhen Liu or Xuanming Shi.

Peer review information *Communications Biology* thanks Robert Maile and the other, anonymous, reviewer(s) for their contribution to the peer review of this work. Primary Handling Editor: Christina Karlsson Rosenthal.